DISTRIBUTION OF GAUSSIAN DECAY FUNCTIONS AND ITS REPRESENTATION BY A COMPRESSED EXPONENTIAL FUNCTION (NMR HAHN-ECHO ANALYSIS OF PPC-COMPOSITES)

[1]Eddy W. Hansen[1,*], Carlos Barreto Soler[2], Xiaoliang Gong[3], Qun Chen[4] & Siw Fredriksen[2]
[1*]Department of Chemistry, UiO, P. O. Box 1033 Blindern, N-0315 Oslo, Norway
[2]Norner AS, Department of Polymer Research, Stathelle, Norway
[3]he School of Electronics and Information Engineering of Tongji University, Shanghai, 201804, P. R. China
[4]Physics Department, Shanghai Key Laboratory of Magnetic Resonance, ECNU, Shanghai 200062, P. R. China

ABSTRACT

It is well known that a stretched exponential function $R_{SEF}(t;q,r^*) = Exp\left[-(r^*t)^q\right]$ for 0 < q < 1 can be expressed by a continuous distribution $P_{SEF}(x,q)$ of single exponential decay functions, i.e.; $R_{SEF}(t;q,r^*) = \int_0^\infty P_{SEF}(x,q)Exp\left[-xr^*t\right]dx$ with $P_{SEF}(s:q) = 1/\pi \int_0^\infty \sin(x^q \sin(\pi q))Exp\left[-x^q \cos(\pi q) - sx\right]dx$. In a recent paper (Hansen et al., *Macromol. Chem. Phys.* **2013**, DOI: 10.1002/macp.201200715) it was suggested that a corresponding compressed exponential function (CEF) $R_{CEF}(t;q,r^*) = Exp\left[-(r^*t)^q\right]$ with $1 < q \leq 2$ can represent a corresponding distribution $P_{CEF}(x,q)$ of Gaussian decay functions; $R_{CEF}(t;q,r^*) = \int_0^\infty P_{CEF}Exp\left[-(xr^*t)^2\right]dx$ with $P_{CEF}(x,q) = 2xP_{SEF}(x^2;q/2)$. Further support and legitimacy of this latter relation is exemplified by numerical calculations ($0 < q < 2$) and its applicability is illustrated by examining the NMR Hahn echo relaxation response of some composite materials of polypropylene carbonates and graphite nano-platelets.

Keywords: *chemistry; compressed-exponential; T_2-distribution; modeling; composites.*

1. INTRODUCTION

It is known that many experimental response functions - as for instance NMR relaxation of fluids confined in porous materials - can be approximated by what is known as a stretched exponential function (SEF) [1 - 6]:

$$R_{SEF}(t;q,r^*) = Exp\left[-(r^*t)^q\right] \quad (1)$$

where t represents time, q is a dimensionless constant restricted to $0 < q \leq 1$ and r^* defines a rate constant of dimension inverse of time. As can be inferred from Equation 1, $t^* = 1/r^*$ defines the time at which the response function R_{SEF} has decayed to e^{-1} of its value at time t = 0.

This type of response function has been interpreted as arising from a continuous distribution $P_{SEF}(t;q,r^*)$ of single-exponential decay functions ($Exp\left[-xr^*t\right]$) with $x = r/r^*$ being a dimensionless parameter. From NMR relaxation- and Pulsed Field Gradient NMR theory, the function $P_{SEF(t;q,r^*)}$ is simply the inverse Laplace transform (ILT) of the response function R_{SEF}:

$$R_{SEF}(t;q,r^*) = Exp\left[-(r^*t)^q\right] = \int_0^\infty P_{SEF}Exp\left[-xr^*t\right]dx \quad (2)$$

In a recent NMR relaxation study on aging of cross-linked polyethylene (XLPE), one of the (three) Hahn-echo relaxation components revealed a q-value equal to approximately 1.3, which was significantly larger than one (1). Hence, this particular Hahn-echo component is unable to be represented by a distribution of single exponential decay functions [7]. Based on some simple mathematical (algebraic) arguments Hansen and coworkers suggested that a distribution $P_{CEF}(x;q)$ of Gaussian decay functions ($Exp\left[-(xr^*t)^2\right]$), defined by:

$$S_G(t;q,r^*) = \int_0^\infty P_{CEF}(x;q)Exp\left[-(xr^*t)^2\right]dx \quad (3)$$

may well be represented by a Compressed Exponential Function R_{CEF}:

$$R_{CEF}(t;q,r^*) = Exp\left[-(xr^*t)^q\right] \quad (4a)$$

with 1 < q < 2 and $P_{CEF}(x;q)$ satisfying the relation:

$$P_{CEF}(x,q) = 2xP_{SEF}(x^2;q/2) \quad (4b)$$

In Ref. 7, $P_{CEF}(s,q)$ was calculated from $P_{SEF}(s,q/2)$ via Equation 4b. However, one important question that was left unanswered and not fully explored was if $S_G(t;q,r^*)$ (Equation 3) strictly equals $R_{CEF}(t;q,r^*)$ (Equation 4a). Hence, in the first part of this work we present some numerical simulations to give additional support and validity of the identity $R_{CEF}(t;q,r^*) = S_G(t;q,r^*)$. Finally, we will exemplify the applicability of equation 3 (and equation 4b) by analyzing the NMR Hahn echo response curve of some certain composite materials made from polypropylene carbonate (PPC) mixed with graphite nano-platelets (GNP).

2. MODEL EVALUATION

2.1. Distribution of Gaussian Functions represented by a Compressed Exponential Function (CEF)

The distribution function $P_{SEF}(s:q)$ can be calculated from the integral formula [8 - 10]:

$$P_{SEF}(s:q) = 1/\pi \int_0^\infty \sin(x^q \sin(\pi q))Exp\left[-x^q \cos(\pi q) - sx\right]dx \quad (5)$$

using MATLAB (version 2010B) and is illustrated in Figure 1A (top) for a series of q-values.

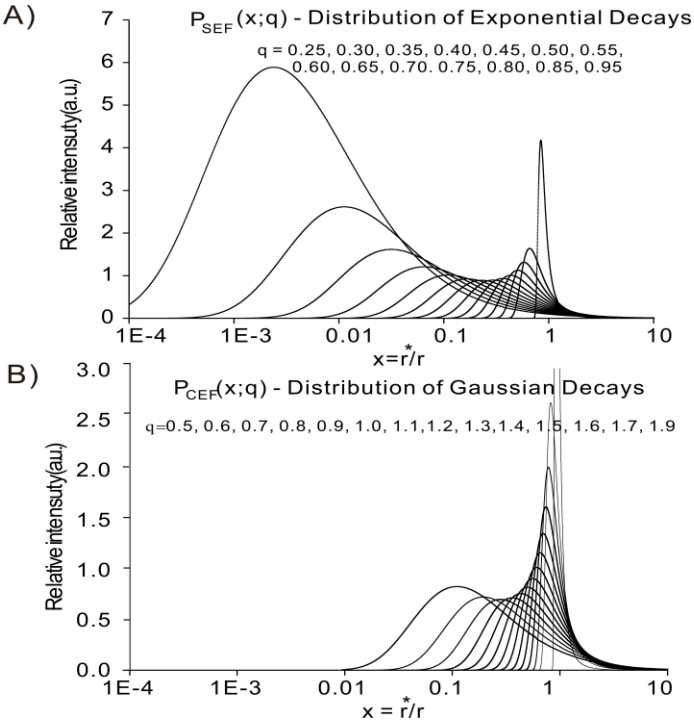

Figure 1. **A**) The distribution $P_{SEF}(x;q)$ of exponential decay functions, as calculated from Equation 5 with q = 0.25, 0.30, 0.35, ..., 0.80, 0.85 and 0.95, and B) the distribution $P_{CEF}(x;q)$ of Gaussian decay functions, as calculated from Equation 4b with q = 0.50, 0.60, 0.70, ...1.60, 1.70 and 1.90, respectively. X is a dimensionless parameter and r^* was arbitrarily set to 0.065. **B**) Corresponding calculations for the distribution function $P_{CEF}(x,q)$ as derived from $P_{SEF}(x,q/2)$ via equation 4b.

2.2 Comparison of $R_{CEF}(t;q,r^*)$ and $S_G(t;q,r^*)$ for a specific r*

The calculation of $S_G(t;q,r_0^*)$ (equation 3) was performed numerically for different t and q values after transforming equation 3 into a finite sum of terms using Microsoft Excel (2010) and keeping r^* fixed ($r^* = r_0^* = 0.065$). As can be inferred from the shape and appearance of the distribution function $P_{CEF}(s;q)$ in Figure 1B (bottom) we found it reasonable to use a logarithmic scaling, by choosing $\ln(x_{n+1}/x_n)$ equal to some constant k in the calculations. Depending on the accuracy of the calculation we found that by setting k ≈ 0.004 the relative difference between $R_{CEF}(t;q,r^*)$ and $S_G(t;q,r^*)$ became less than 0.2% for all q. Importantly, this difference could be reduced and thus improved by choosing a smaller value of k. The excellent agreement between the two expressions is illustrated on Figure 2 which represents a visual confirmation of this equivalence, i.e., $R_{CEF}(t;q,r^*) = S_G(t;q,r^*)$.

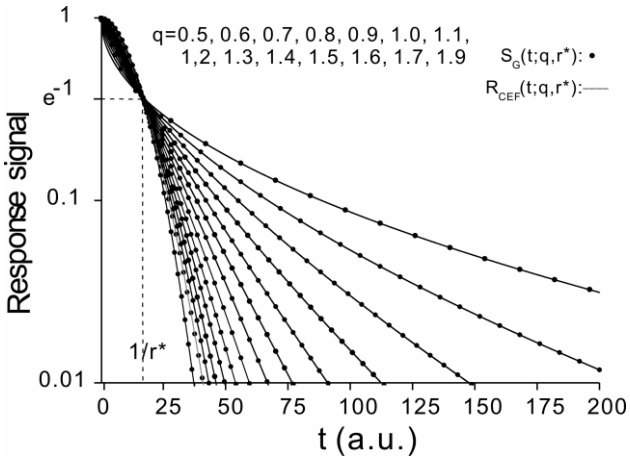

***Figure 2**. The integral function $S_G(t; q, r^*)$ (equation 3) and the response function $R_{CEF}(t;q,r^*)$ (equation 4a) as a function of time t for q (left to right) = 0.50, 0.60, … ,1.60, 1.70 and 1.90 and r set arbitrarily to 0.065. All curves go through the point $(1/r^*, e^{-1})$.*

2.3 Comparison of $R_{CEF}(t;q,r^*)$ and $S_G(t;q,r^*)$ for arbitrary r*

In the previous section it was shown that:

$$S_G(t;q,r_0^*) = \int_0^\infty P_{CEF}(u/r_0^*;q)\exp\left[-((u/r_0^*)\cdot r_0^* t)^2\right]d(u/r_0^*) = R_{CEF}(t;q,r_0^*) = \exp\left[-(r_0^* t)^q\right] \quad (6)$$

which, according to equation 3, can be written:

$$S_G(t;q,r^*) = \int_0^\infty P_{CEF}(z/r^*;q)\exp\left[-((z/r^*)\cdot r^* t)^2\right]d(z/r^*) \quad (7)$$

By substituting z/r^* with u/r_0^* in equation 7 we obtain:

$$S_G(t;q,r^*) = \int_0^\infty P_{CEF}(u/r_0^*;q)\exp\left[-((u/r_0^*)\cdot(r^* r_0^*/r_0^*)\cdot t)^2\right]d(u/r_0^*)$$

$$= \int_0^\infty P_{CEF}(u/r_0^*;q)\exp\left[-((u/r_0^*)\cdot(r_0^*(r^*/r_0^*)\cdot t)^2\right]d(u/r_0^*) \quad (8)$$

$$= \int_0^\infty P_{CEF}(u/r_0^*;q)\exp\left[-((u/r_0^*)\cdot(r_0^* t')^2\right]d(u/r_0^*)$$

Where we have introduced $t' = r^* t / r_0^*$. By reference to equation 6 we may express equation 8 as:

$$S_G(t;q,r^*) = R_{CEF}(t';q,r_0^*) = \exp\left[-(r_0^* t')^q\right] = \exp\left[-(r_0^* \cdot (r^* t / r_0^*)^q\right] = \exp\left[-(r^* t)^q\right] = R_{CEF}(t;q,r^*)$$

showing that $R_{CEF}(t;q,r^*)$ is equivalent to $S_G(t;q,r^*)$ for arbitrary r^*. Hence, a change in r^* simply corresponds to a scaling of the time parameter t by a factor r^*/r_0^* .

In the next section we will apply equations 3 and 4 to derive the proton spin-spin relaxation rate distribution of various composite materials prepared from mixtures of polypropylene carbonate and graphite nano-platelets from NMR Hahn echo measurements.

3. PROTON SPIN-SPIN RELAXATION TIME DISTRIBUTION OF PPC-COMPOSITES THEORETICAL OUTLINE AND COMMENTS

The graphite nano-platelets within a melt modified (PPC) composite introduce a surplus of "cross-links" and/or entanglements (chemical and/or physical cross links) as illustrated in Figure 3.

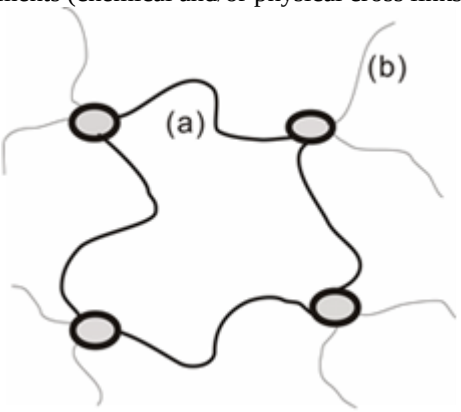

Figure 3. *The graphite nano-platelets within a melt modified (PPC) composite introduce additional "cross-links" and/or entanglements (chemical and/or physical cross links).*

From an NMR point of view this type of morphology generates liquid-like (high molecular mobility) and solid-like (slow molecular mobility) domains within the sample. The fast molecular motion averages the dipolar coupling and is responsible for the liquid-like behavior. The anisotropic molecular motion which originates from cross-linking and topological constraints, lead to a non-averaging of the dipolar coupling which results in the NMR solid-like behavior. As a consequence, the molecular motion becomes more restricted and solid-like as the number of cross-links increases. Hence, the following motional characteristics may be distinguished: 1) A fast local segmental motion that is described by a correlation time τ_f. Due to its anisotropy, as caused by cross-linking, a non-averaged dipolar interaction M_2 results, which is quantified by an anisotropy parameter q according to:

$$M_2 = qM_{2,rl} \quad (9)$$

where $M_{2,rl}$ is the rigid-lattice second moment. Two other types of slow motions are the reptation (chain folding fluctuations) and the tube renewal motion [11]. Both of these motions are slow isotropic motions, characterized by a correlation time τ_s, and cannot be distinguished.

Anyhow, without going into further details Anderson and Weiss have derived a model equation which is frequently adopted in the analysis of anisotropic motions of network which takes the form [12]:

$$I(t) = I_0 \exp\left[- M_{2,rl}\tau_f t - qM_{2,rl}\tau_s^2\left[\exp(-t/\tau_s) + t/\tau_s - 1\right]\right] \quad (10a)$$

and is denoted the AW-equation. In general, it is expected that the transversal relaxation be described by a sum of three (3) such terms (Equation 10a), originating from crosslink chains, dangling chain ends and "sol" chains, respectively. However, the "sol"-term results in a single exponential relaxation behavior. The "dangling chain end"-term may reveal some small anisotropy q', however, this will depend on the actual polymer system [13]. A preliminary analysis of the data in Figure 4 revealed only one AW-term in addition to a single exponential term. In particular, we found that the three terms $M_{2,rl}$, τ_s and q could not be reliably distinguished and is most probably due to the correlation time τ_s of the slow motion being longer (on the NMR time scale; $\tau_s >> t$) than the relaxation time of the magnetization, i.e.,

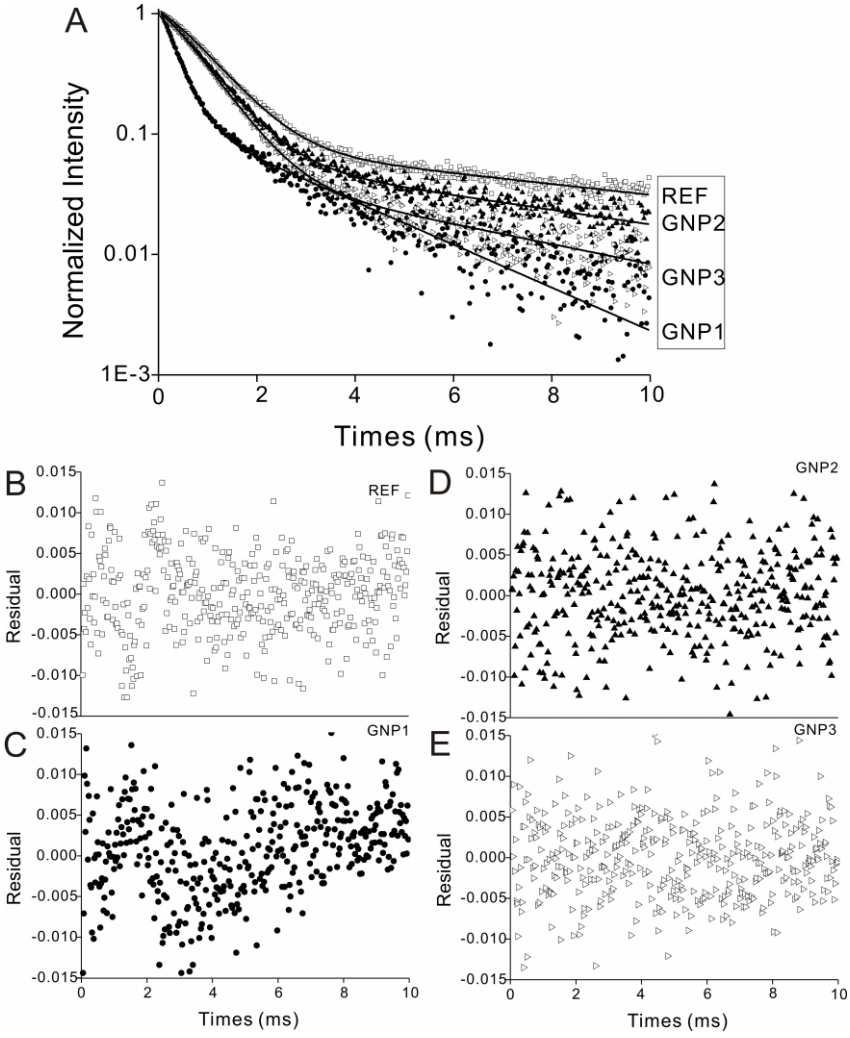

Figure 4. *Observed Hahn echo decays of samples REF, GNP1, GNP2 and GNP3 acquired at 90C. REF represents a PPC reference sample and GNP1 - 3 are PPC composites containing 10wt% of different types of graphite Nano platelets. The solid curves represent non-linear least squares fits to Equation 9. The bottom figures (B – E) show the residual curves for each individual sample .*

the rigid lattice limit is approached ($M_{2,rl} \cdot \tau_s >> 1$). As a consequence (after Taylor expanding the exponential term in equation 10a) equation 10a may be reformulated to read:

$$I(t) = I_0 \exp\left[- M_{2,rl}\tau_f t - (qM_{2,rl})t^2\right] \quad (10b)$$

From general NMR theory, the second moment M_2 (equation 9) is associated with the spin-spin relaxation rate R_2 according to: $R_{21} = M_{2,rl}\,\tau_f$ and $R_{22} = \sqrt{qM_{2,rl}}$ which inserted into Equation 10b read:

$$I(t) = I_0 \exp\left[- R_{21}t - (R_{22}t)^2\right] \quad (10c)$$

where R_{21} and R_{22} are the spin-spin relaxation rates associated with the fast and slow motions, respectively. Equation 10c has been successfully applied by A. Voda on the relaxation time analysis of carbon black filled EDPM samples [14]. When model fitting equation 10c to the data in Figure 4 it was found that only the second term was of significance.

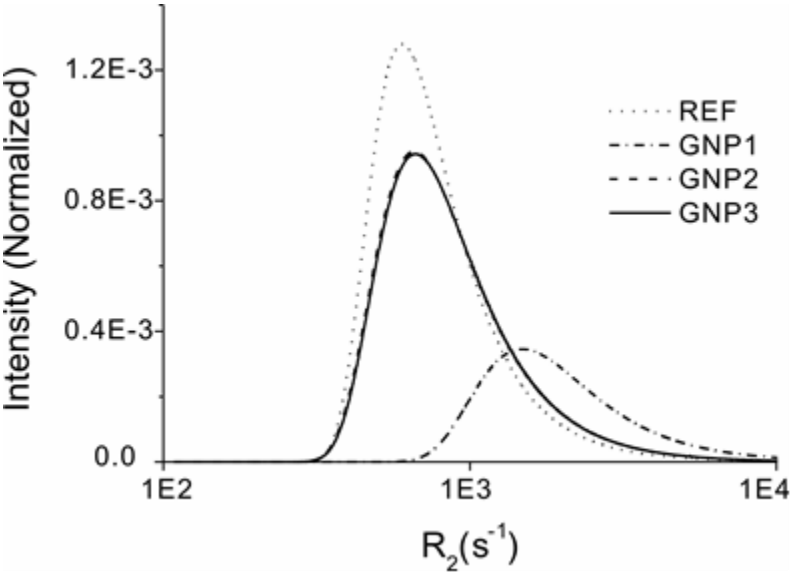

Figure 5. *Spin-spin relaxation distribution of samples REF, GNP1, GNP2 and GNP3. Details regarding these calculations are discussed in the theory section.*

Since the composite materials are inherently heterogeneous we find it reasonable to introduce a distribution $f(R_2)$ of relaxation rates R_2. Hence, the transversal magnetization $I(t)$ was represented by a sum of Gaussian functions, according to:

$$I(t) = \sum_i f(R_{2i}) \exp\left[-(R_{2i}t)^2\right] \quad (11)$$

From the theoretical outline discussed in section 2, it foolows that the normalized relaxation function $I(t)$ can be writtwn:

$$I(t) = f_A \exp\left[-(R_{2A}t)^q\right] + (1 - f_A)\exp(-R_{2B}t) \quad (12)$$

where the first term represents a CEF with an exponential factor q ($1 < q < 2$). The second term represents the relaxation contribution from other sources (for instance the sol fraction) which - for simplicity - is assumed to be represented by a single exponential function with a spin-spin relaxation rate R_{2B}. The relative fraction of component A is denoted f_A. As a consequence, the relaxation model contains a total of four (4) adjustable parameters. It must be emphasized that a similar formula (equation 12) was adopted phenomenologically by Litvinov and coworkers in their analysis of

rubber-filler interactions and network structure in relation to stress-strain behavior of vulcanized, carbon black filled EPDM [15]. However, they did not comment on any possible relaxation distribution but applied equation 12 simply as a convenient fitting function.

4. EXPERIMENTAL

4.1 Material preparation

The GNP/PPCPA (graphene nanoplates/polypropylene carbonate modified with pyromellitic dianhydrid) composites were prepared in two compounding steps from unmodified PPC. In the first step, a melt modification with PDAH was performed on PPC to obtain the PPCPA matrix. As a second step, the GNP particles were melt compounded into PPCPA.

i) Preparation of PPCPA: PPCPA was prepared from a commercial grade of PPC (QPAC40 from Empower Materials, USA); PPC was characterized: T_g (midpoint): 21.4°C (DSC); cyclic propylene carbonate (CPC): 4.8 % (FTIR calibrated from ^{1}H-NMR); M_w: 184.000, *PDI*: 5.1 (SEC in THF, PS standards). PPC pellets were dried under dry N_2 atmosphere at 25°C for 72 h and compounded with 0.4 wt% PDAH (97 % from Sigma Aldrich) in a pilot Prism 24 twin screw compounder (Barrel D: 24 mm, L/D: 25, feeding speed: 6 kg/h, screw speed: 300 r.p.m, average barrel and die temperature: 140°C). The extrudate was cooled by water, cut into pellets and dried under dry N_2 by a strand pelletizer.

ii) Melt compounding GNP into PPCPA: PPCPA was milled and hand mixed with GNP. Three hundred grams of each recipe was fed into a pilot Prism 16 twin screw compounder (Thermo Fisher Scientific, DE, Barrel D: 16 mm, L/D: 25, feeding speed: 2 kg/h, screw speed: 500 r.p.m, average barrel and die temperature: 140°C). The extrudate was cooled by water, cut into pellets and dried under dry N_2 by a strand pelletizer. The initial and final portions of the extrudate were discarded, and approximately 120 g of each recipe was collected.

Three grades of GNP were selected for this study and purchased from XGSciences (USA). Characteristics of the GNPs, as given by the manufacturer, are provided in table 1.

Table 1. GNP grade and basic characteristics supplied by XG Sciences (producer)

Abbr.	Grade	S/V[1] (m^2/g)	d[2] (nm)	2R[3](µm)	Carbon content (wt%)
GNP1	xGNP M15	150	6	15	
GNP2	xGNP M25	120	6	25	99,50
GNP3	xGNP C500	500	2	<2	

[1] Specific surface area, [2] Average particle thickness, [3] Average particle diameter.

4.2 Experimental Techniques

4.2.1 Rheology: Shear storage and loss modulus, *G'* and *G''*, were measured within the linear viscoelastic range using the Rheometrics Scientific RDA II Analyzer, equipped with plate-plate geometry (diameter 25 mm), on hot pressed specimens. A preheating time of 200 s was used, as well as an angular frequency (ω) interval 0.06 to 15.85 rad/s for isothermal/isostrain measurements at 140°C / 10 %.

4.2.2 NMR: The proton Hahn-echo experiments were performed at 90^0C (which is well above the glass transition temperature of approximately 40^0C), on a Maran Ultra NMR instrument operating at 20 MHz proton frequency. The dwell time was set to 0.1 µs and a total of 8 transients were sampled for each τ. The repetition time was set to 5 s which is more than five times the spin-lattice relaxation time and ensures quantitative sampling of the echo. The echo intensity was determined from an average of 10 data points (out of 512 points defining the echo) around the echo maximum. The echo intensity was samples at 400 different echo times (τ) in which τ was increased systematically from 0.025 ms to 5 ms. The 90^0-rf-pulse was set to 2.15µs.

5. RESULTS AND DISCUSSION

The observed echo response curve (relaxation curve) of all four samples (REF, GNP1, GNP2 and GNP3) is shown in Figure 4 and clearly signifies a multi-component behavior. The solid curves were model-fitted to Equation 12 and each residual curve (Figure 4B – E) reveals clearly a random error distribution. The parameters in Equation 12, as obtained from a non-linear model-fitting to Equation 12, are summarized in Table 2 and reveal all a high quality, as noticed from their small standard error. Also, the average value $R_{2A,average}$ of each relaxation distribution $f(R_{2A})$ of component A (Figure 5) can be easily calculated from the well-known properties of a stretch exponential function:

$$R_{2A,average} = R_{2A}\,\frac{\Gamma(q)}{q} \qquad (13)$$

where Γ is the gamma function, or the factorial function. These parameters are also tabulated in Table 2
According to the model developed in the first part of this work (Equations 3 and 4) we can plot the relaxation rate distribution curve $f(R_{2A})$ which represents a spin-spin relaxation rate "fingerprint " of component A. These fingerprints are illustrated on Figure 5 for all four (4) samples.
We should emphasize that the q-factor in the Compressed Exponential Function (CEF) is a distribution width indicator and attains the value 2 for a single Gaussian function, which is then represented by a δ-function. The distribution width increases as q decreases towards 1 and is illustrated by reference to the actual relaxation distributions in Figure 5 and their corresponding q parameter (Table 2).

As can be inferred from the spin-spin relaxation distribution curves $f(R_{2A})$ in Figure5 and the corresponding data in Table 1, samples GNP2 and GNP3 are practically equal (all corresponding parameters between the two samples differ by less than 2.5% and is statistically insignificant) except for the relaxation rate R_{2B} which is faster by about 40% in GNP3, suggesting the molecular motion within domain B to be more constraint in sample GNP2. Also, asmall, but significant difference is noticed between their q-parameter, suggesting the R_2-distribution of GNP 2 to be slightly broader than in GNP3.

We remark that the average relaxation rate $R_{2A,\ average}$ is systematically smaller than R_{2A} by approximately 25%, as can be inferred from Figure 6 (Left), and originates from a skewness of the distribution.

In contrast, sample GNP1 reveals NMR characteristics (Table 2) that are significantly different from both the reference sample REF and samples GNP1 and GNP2. The exact reason for this behavior is difficult to rationalize from the sample characteristics of the different GNP samples (Table 1), and suggests that the explanation must be sought in the specific chemistry and physics that operate during the processing of the samples.

It is particularly encouraging, however, to see the strong correlation between the NMR relaxation rates ($R_{2A,\ average}$, $R_{2B)}$ and the rheology parameter $x = \Delta\log G / \Delta\log\omega$ (Figure 6; Right), which – not too surprisingly – suggests that cross-linking plays a major role [12 - 15].

5.1 Distribution of Gaussian Functions represented by a CEF

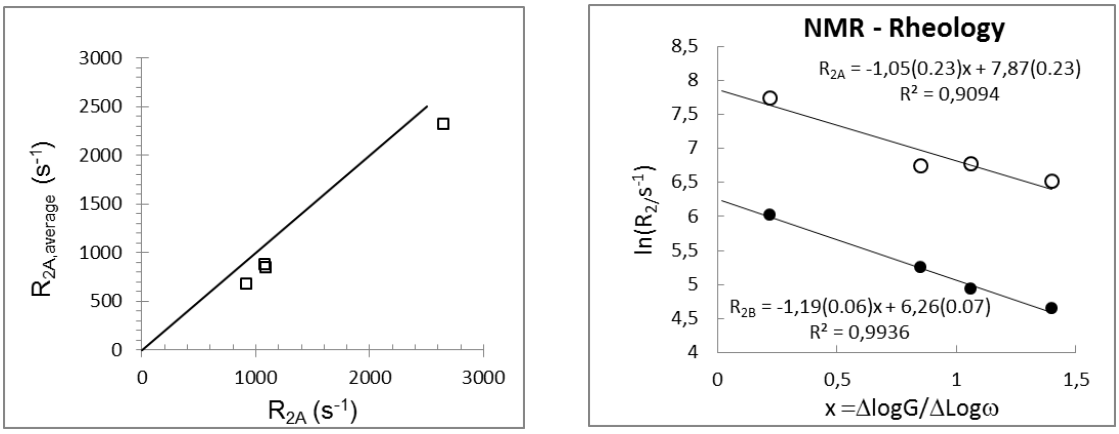

***Figure 6 Left)**. Relation between relaxation rate R_{2A} (Equation 12) and its average value*

*$R_{2A,\ average}$, as determined from the relaxation rate distribution (Figure 5) via Equation 13. The dotted line represents $R_{2A,\ average} = R_{2A}$. **Right)**. Relation between NMR spin-spin relaxation rate R_2 and the rheology parameter $x = \Delta \log G / \Delta \log \omega$ where G is the shear storage module storage and ω is the circular frequency.*

Table 2. NMR characteristics of samples REF, GNP1, GNP2 and GNP3 as derived by model-fitting Equation 12 to the observed Hahn echo response curves (Figure 4).

Parameter	**REF**	**GNP1**	**GNP2**	**GNP3**
f_A(%)	91.5 ± 0.5	87.2 ± 0.5	93.1 ± 0.3	94.5 ± 0.6
$R_{2A}(s^{-1})$	916 ± 6	2650 ± 11	1080 ± 11	1090 ±12
Q	1.292 ±0.007	1.108 ± 0.015	1.194 ± 0.004	1.230 ± 0.006
$R_{2A,av}(s^{-1})$[1)]	679 ± 4	2314 ± 10	870 ± 9	848 ± 9
R_{2B} (s^{-1})	104 ± 1	412 ± 2	139 ± 1	191 ± 1

[1)] Calculated from Equation 13

It is exciting to see – within experimental error – that the slope of R_2 vs. x is the same for both components A and B. However, it is outside the scope of this work to discuss these – although important aspects – further. Additional experimental work is needed and we are - at present - designing such experiments which will involve both NMR and other experimental techniques in combination. In particular, Equation 12 will represent an important and major tool in the analysis.

6. CONCLUSION

Numerical calculations show that for $0 < q < 2$, the function $R_{CEF}(t; q, r^*) = \exp\left[-(r^* t)^q\right]$ can be represented by a continuous distribution $P_{CEF}(x; q)$ of Gaussian functions, according to the relation: $R_{CEF}(t; q, r^*) = \int_0^\infty P_{CEF}\, Exp\left[-(xr^* t)^2\right] dx$ where $R_{CEF}(t; q, r^*)$ satisfies the equation: $P_{CEF}(x, q) = 2x P_{SEF}(x^2; q/2)$ and $P_{SEF}(s : q) = 1/\pi \int_0^\infty \sin(x^q \sin(\pi q)) Exp\left[-x^q \cos(\pi q) - sx\right] dx$. In particular, it is illustrated how this function can be a helpful and efficient tool when analyzing experimental Hahn echo relaxation responses from PPC and PPC-composites.

7. ACKNOWLEDGEMENT

Eddy Hansen wants to thank Prof. Qun Chen at the Physics Department and Shanghai Key Laboratory of Magnetic Resonance, East China Normal University for financial support and generosity and for inviting me to stay at ECNU during the last part of this project.

8. REFERENCES

[1] J. Tritt-Goc, N. Piślewski, S. Kościelski, F. Mila, *Cement and Concrete Research* 2000, 30, 931.

[2] N. Nestle, *Cement and Concrete Research* 2004, 34, 447.

[3] A. Narayanan, J. S. Hartman, A. D. Bain, *J. Magn. Res.Ser. A* 1995, 112, 58,

[4] R. L. Magino, W. Li, M. P. Velasco, J. Trujillo, D.A. Reiter, A. Morgenstern, R. G. Spencer, *J. Magn. Res.* 2011, 210, 184.

[5] P. J. Prado, B. J. Balcom, S. D. Beyea, T. W. Bremner, R. L. Armstrong, R. Pishe, P. E. Gratten-Bellew, *J. Phys. D: Appl. Phys.* 1998, 31, 2040.

[6] X. Gong, E. W. Hansen, Q. Chen, *Macromolecular Chemistry and Physics* 2012, 278.

[7] E. W. Hansen, X. Gong and Q. Chen, *Macromolecular Chemistry and Physics* 2013, DOI: 10.1002/macp.201200715.

[8] H. Pollard, *Am. Math. Soc.* 1946, 52, 908.

[9] C. P. Lindsay, G. D. Patterson, *J. Chem. Phys* 1980, 73, 3348.

[10] M. N. Berberan-Santos, *J. Math. Chem.* 2005, 38, 165.

[11] P. G. de Gennes, *J.Chem Phys.*, 1971, 55, 572.

[12] P. W. Anderson, P. R. Weiss, *Rev. Mod. Phys.* 1953, 25, 269.

[13] U. Heuert, M. Knørgen, H. Menge, G. Scheler and H. Schneider, *Polymer Bulletin*, 1996, 37, 489.

[14] A. E. Voda, PhD-dissertation ("Low Field NMR for Analysis of Rubbery Polymers", 2006, Aachen, Techn. Hochsch, identifier; urn:nbn:de:hbz:82-opus-14288)

[15] V. M. Litvinov, R. A. Orza, M. Klüppel, M. van Duin and P. C. M. M. Magusin, *Macromolecules*, 2011, 44, 4887.